EFDA–JET–PR(12)37

P.A. Schneider, E. Wolfrum, R.J. Groebner, T.H. Osborne, M.N.A. Beurskens,
B. Kurzan, T.Pütterich, E. Viezzer, the ASDEX Upgrade Team,
the DIII-D Team and JET EFDA contributors

Analysis of Temperature and Density Pedestal in a Multi-Machine Database

Analysis of Temperature and Density Pedestal in a Multi-Machine Database

P.A. Schneider[1], E. Wolfrum[1], R.J. Groebner[2], T.H. Osborne[2], M.N.A. Beurskens[3], B. Kurzan[1], T.Pütterich[1], E. Viezzer[1], the ASDEX Upgrade Team[1], the DIII-D Team[2] and JET EFDA contributors*

JET-EFDA, Culham Science Centre, OX14 3DB, Abingdon, UK

[1]Max-Planck-Institut für Plasmaphysik, EURATOMAssociation, Garching, Germany
[2]General Atomics, PO Box 85608, San Diego, CA 92186-5608, USA
[3]EURATOM-CCFE Fusion Association, Culham Science Centre, OX14 3DB, Abingdon, OXON, UK
** See annex of F. Romanelli et al, "Overview of JET Results",*
(23rd IAEA Fusion Energy Conference, Daejon, Republic of Korea (2010)).

Preprint of Paper to be submitted for publication in
Nuclear Fusion

ABSTRACT

A comparison of the AUG and DIII-D temperature pedestals showed significant differences between electrons and ions. For high collision rates the ions are coupled to the electrons and show very similar pedestal top values and gradients. For lower collision rates both decouple and the ion pedestal becomes less steep. The electron temperature gradient scales linearly with its pedestal top value. This trend is independent of collisionality and plasma shape. The normalized total pressure gradient shows strong correlations with the plasma shape in a way expected by peeling-ballooning theory. The different behaviours of the electron temperature gradient only and the total pedestal pressure gradient suggests a limit for the electron temperature pedestal different from linear edge MHD stability.

1. INTRODUCTION

The high confinementmode (H-mode) in tokamak plasmas is one of the favoured scenarios for future fusion devices. In order to document and understand the features of the H-mode it is mandatory to analyse a wide range of different plasma parameters. One way to achieve this is to compare tokamak devices with different capabilities. In the presented study data is included from ASDEX Upgrade (AUG), DIII-D and JET. Together they cover different machine sizes and thus minor radii $a \in [0.47, 0.91]$ m, a wide range of plasma current $I_p \in [0.5, 2.7]$ MA, toroidal magnetic field $B_t \in [0.7, 2.8]$ T, plasma shape and kinetic plasma properties.

Particularly important in an H-mode plasma is the edge pedestal which is responsible for a significant fraction of the plasma stored energy [1–3]. In the recent years a lot of effort was focused on documenting and understanding the basic properties of the pedestal - its gradients [2, 4, 5], widths [6–12] and top values [13–15].

This paper focuses on the pedestal characteristics just before the onset of an edge localized mode (ELM) in type-I ELMy H-modes. The analysis in this paper is based on a database obtained with the two-line pedestal characterisation which is described in [12] along with the definitions of the parameters used in this paper. The focus is put on gradients in the pedestal. In Section it is shown that gradients of T_e and T_i at the outer midplane behave differently. JET was not included in studies of ∇T_i because no ion temperature data was available for the pedestal. In Section the density and pressure gradients are discussed. In Section the different correlations of the normalized total pressure gradient are illustrated. In particular, a strong correlation with the plasma shape is observed.

2. SEPARATION OF ELECTRONS AND IONS

AUG and DIII-D have fairly similar specifications concerning their engineering parameters a, B_t and I_p. One significant difference between the two machines is the material of the first wall. The plasma facing components of AUG are covered with tungsten (W) while in DIII-D they are made out of carbon (C). In a recent comparison of AUG data with and without the complete W wall [16] it was shown that, besides similar discharge parameters and no gas puffing, the electron pedestal top temperature $T_{e,ped}$ and density $n_{e,ped}$ vary significantly depending on the wall material. With a

W first wall the density is increased by 10-20% while at the same time the temperature decreases so a similar electron pressure $p_{e,ped}$ is obtained. The mechanism causing this effect is not clear, but it results in a significant increase of the electron collisionality ν_{e*} for plasmas in AUG with full W wall compared to discharges with a partial carbon wall and otherwise identical discharge parameters. This phenomenon helps to explain the different collisionality regimes observed for AUG ($\nu_{e*} \in [0.3,3.8]$) and DIII-D ($\nu_{e*} \in [0.02, 0.8]$). Before the upgrade to a full W wall in AUG, it was possible to reach collisionalities as low as observed in DIII-D. However, these data cannot be included in the following analysis because the high resolution edge charge exchange recombination CER diagnostic [17], which is capable to measure ion temperature gradients in the pedestal, was only installed after the wall upgrade. One has to keep in mind that the CER diagnostic measures the temperature of impurity ions. Fast energy transfer rates between impurity and main ions suggest both are coupled, measurements of the core plasma confirm this assumption [18], but there is no experimental confirmation in the pedestal region.

Temperature gradients of electrons and ions show different behaviour for AUG and DIII-D. In Fig.1 the pedestal gradient of T_e and T_i is plotted against the temperature at the electron pedestal top. The gradients shown here represent the mean slope in the steep pedestal region. In the case of AUG (a) electron and ion temperature show a comparable relation between pedestal top value and gradient. For DIII-D (b) the ion temperature gradient is significantly lower than ∇T_e for comparable temperatures. The reason for the different observations at AUG and DIII-D might be connected with the collision rates in the plasma. However, the presented data does not allow to give a final answer to this question.

The observations suggest a change in the balance of electron and ion heat channels. This could also be explained with higher collision rates at AUG, where the ion temperature is linked with the electron temperature. The profiles of T_e and T_i can show similar pedestal gradients and pedestal top values. For lower collision rates, as is the case for DIII-D, ∇T_i can significantly differ from ∇T_e. This implies that the heat transfer between electron and ion channels is not fast enough to guarantee their equilibration and that the electron and ion gradients are set by different physical mechanisms.

Further observations suggest that the ion temperature can be set by the electrons and that the electron temperature is fairly independent of the ions. Fig.2 (a) shows that the electron temperature gradient scales linearly with Te,ped, this relation is observed independently of variations in machine size, plasma shape, heating power, electron density and ion temperature. Since there is no density dependence at constant $T_{e,ped}$ there is also no direct collisionality dependence, only an indirect correlation due to the T_e dependence in ν_{e*}. This is consistent with observations of the T_e and n_e pedestal width where no significant dependence on collisionality was reported [6, 7, 9–12]. The ion temperature gradient shown in Fig.2 (b) exhibits a much larger scatter for one pedestal top value than the electron temperature. This scatter does not appear for AUG discharges with high collision rates, Fig.1 (a), and therefore, suggests a stronger coupling between electron and ion heat channels in this case.

3. ELECTRON DENSITY AND PRESSURE GRADIENTS

The gradient in the pedestal of the electron density also shows a correlation with the pedestal top value which is consistent for all machines. However, as is illustrated in Fig.3 (a) the distribution of the measurements is much broader than it was for the temperature. For AUG and JET the external gas puff can influence the correlation of gradient and pedestal top. With larger gas puff higher pedestal top values are obtained while the gradient remains unchanged. After aligning the profiles to the separatrix position determined by the temperature a similar result is obtained for AUG and JET Fig.4. The gas puff causes an increase of the separatrix density and the whole profile is shifted to higher densities with roughly constant width, where the width is defined from the pedestal top up to the separatrix. For AUG the increase in density at the separatrix and in the SOL is even more pronounced than at JET. This also indicates the different absolute impact of the gas puffing and confirms that external gas puffing cannot be used as comparable quantity in inter machine comparisons. The gas puffing at DIII-D is considerably lower – typically 20–30% of a gas puff in AUG - and does not show any influence on the pedestal top density in the presented data set. The alignment of the profiles was crosschecked with measurements of the divertor radiation which suggest higher neutral density in the divertor for both high fuelling cases compared to the low fuelling cases. This means a higher separatrix density is expected with increased fuelling and is consistent with the separatrix position obtained from the temperature profiles.

The gradient of the pedestal pressure in Fig.3 (b) also shows a strong correlation with the pedestal top value. For all three machines the measurements are distributed around a gradient-top ratio which would correspond to a pedestal width of ~1.5cm and does not show systematic deviations. In particular, no influence of the machine size is observed in the JET data (green triangles).

4. NORMALIZED PRESSURE GRADIENT

For edge stability analysis a different representation of the gradients is of interest. This is the normalized total pressure gradient which is used with the definition of Ref. [19] Eq. (42). α arises from the energy balance between destabilising energy available due to the gradient of the total pressure $p = p_e + p_i$ and the energy required for field line bending.

The ELM instability is currently best described with the peeling-ballooning theory [20] where a critical value of the edge current density j and the normalized pressure gradient cause a combined peeling-ballooning mode to become unstable. For a given plasma discharge a stability boundary can be illustrated in a j–α diagram. For most published cases of type-I ELMy H-modes the experimental point lies near the peeling-ballooning stability boundary [9, 21–24]. The position of the boundary in a j–α diagram varies with plasma parameters as does the location of the operational point on this boundary. Often discussed quantities are the plasma collisionality, the plasma shape and the magnetic shear at the edge. The information obtained with the AUG, DIII-D database about the correlations of with these parameters is documented in the remainder of this section.

Because of the differences in the ion and electron temperatures the approximation $p = 2p_e$ is not used. To account for the differences in the temperature gradients the following approximation is applied

$$\frac{\partial p}{\partial \Psi} \sim \left(1 + \frac{1}{2}\frac{\frac{\partial T_i}{\partial \Psi}}{\frac{\partial T_e}{\partial \Psi}} + \frac{1}{2}\frac{T_{i,ped}}{T_{e,ped}}\right)\frac{\partial p_e}{\partial \Psi}. \quad (1)$$

This approximation implies a constant pedestal width of T_e and n_e in real space coordinates, considering Fig.2 (a) and Fig.3 (a) this is a reasonable assumption. Further, an effective charge number $Z_{eff} = 1$ is used. In principle, a Z_{eff} profile to determine ni would be preferable. However, due to the large uncertainties of Z_{eff}, particularly at the edge, its inclusion would not improve the approximation for ∇p. To quantify the possible error due to this approximation Z_{eff} was varied by a factor of 4 and the change of was calculated. In spite of the large variation in Z_{eff} changed by less than 30%. When comparing quantities which are similarly affected by Z_{eff} the deviation from the correct values becomes even less.

The plasma shape divides the data set in two different regions, one of weak shaping and another of strong shaping. In Fig.5 the collisionality dependence of α is shown for different triangularity. For low triangularity (a) only α values below 6 are reached. There is one exception which reaches $\alpha > 9$, however, this is the only discharge in the set with a relatively large elongation of $\kappa > 1.85$ and therefore also strongly shaped compared to a circular cross section. For high triangularity (b) larger values of α are possible, at the same time no correlation with collisionality is observed.

Another parameter which correlates with the normalized pressure gradient is $f_q = q_{95}/q_{cyl}$. With increasing fq also larger values of are possible as shown in Fig.6 (a). Two regions can be identified, one where f_q increases but varies little ($f_q < 1.5$) and another were strongly increases with f_q ($f_q > 1.5$). These regions also coincide with the regions of different shape in Fig.5. In Fig.6 (b) f_q is compared to the collisionality and both parameters do not show a notable correlation. Rather, a wide range of collisionalities can be covered while keeping f_q constant. The physical meaning of f_q is not perfectly clear. f_q is correlated with p,ped, however, not equivalent [12]. One possibility is that f_q is an estimate of the edge current density; while βq_{cyl} represents the inverse of the total plasma current, q_{95} excludes the outer 5% of the plasma radius and can be accurately determined by equilibrium reconstruction codes [25]. Therefore, f_q could be a measure for the relative edge current density. In this case Fig.6 (a) would suggest a strong link of the normalized pressure gradient and the edge current density, which can change the local shear significantly.

To assess the influence of the collisionality on the edge current density and understand Fig.6 (b) it is useful to study the bootstrap current. With larger collisionality the bootstrap drive coefficients decrease [26]. However, this does not necessarily mean smaller bootstrap contribution to the edge current density. In contrary, j_{boot} can even increase slightly. Following the ideas in [26], a simple estimate can be made. Assuming constant pressure and proportionality between gradients and pedestal height, a change of the collisionality from 0.5 to 1.7 will influence the bootstrap current by less than 5%. This is because of the stronger boostrap drive due to the density compared to the temperatures which compensates the overall reduction in the drive coefficients. Therefore, no distinct conclusion may be drawn from changes in collisionality to changes in bootstrap current. It depends strongly on how the variation in collisionality is achieved. For example, varying ν_{e*} with strong gas puffing

will break the assumption of proportionality between gradients and pedestal height as discussed in Section and most likely change the bootstrap current.

CONCLUSION

Surprisingly, the real space electron temperature gradient shows a linear dependence on $T_{e,ped}$, thus $T_{e,ped}/\nabla T_e \sim$ const. The dependence of these two parameters is not disrupted by changes in plasma current, magnetic field, plasma shape or collisionality. The ion temperature gradient does not show such a linear dependence with the pedestal top value but exhibits significant deviations betweenmachines whichmight be connected to different collisionality in the investigated plasmas. Changes in gas puffing have no impact on the electron density gradient, while the density pedestal top can be influenced by the gas-puff in a certain fuelling rate interval which differs for the machines. Also the electron pressure gradient appears to be independent of collisionality and plasma shape.

The normalized pressure gradient α, which contains information of electrons and ions, does not exhibit a clear dependence on a single parameter, as was the case for the electron channel alone. A clear separation of high and low α is possible with the plasma shape, where high α are only achieved with strong shaping. There are indications that large elongation also opens up the access to high as it is observed for the triangularity in the presented data set and previous studies [27]. Both can be expected from the peelingballooning theory [28, 29].

The different observations favour various mechanisms. The pedestal top values of electron and ion temperature and density can be individually transport limited, but together they still reach the peeling-ballooning stability limit.

ACKNOLEDGEMENTS

The authors want to thank P.J. McCarthy for valuable discussions on the plasma equilibrium and also H. Zohm, K. Lackner and P.B. Snyder for their valuable input. This work was supported in part by EURATOM and carried out within the framework of the European Fusion Development Agreement. The views and opinions expressed herein do not necessarily reflect those of the European Commission. This work was supported in part by the U.S. Department of Energy under DE-FC02-04ER54698 and DE-FG02-95ER54309.

REFERENCES

[1]. Suttrop, W. et al., Plasma Physics and Controlled Fusion **39** (1997) 2051.
[2]. Groebner, R.J. et al., Plasma Physics and Controlled Fusion **48** (2006) A109.
[3]. Maggi, C.F., Nuclear Fusion **47** (2007) 535.
[4]. Groebner, R.J. et al., Nuclear Fusion **50** (2010) 064002.
[5]. Burckhart, A. et al., Plasma Physics and Controlled Fusion **52** (2010) 105010.
[6]. Osborne, T.H. et al., Characteristics of the H-Mode Pedestal and Extrapolation to ITER, in Proceedings of the 19th IAEA Conference, pages IAEA–CN–94/CT–3, 2002.
[7]. Hughes, J. W. et al., Physics of Plasmas **9** (2002) 3019.

[8]. Urano, H. et al., Nuclear Fusion **48** (2008) 045008.
[9]. Maggi, C. et al., Nuclear Fusion **50** (2010) 025023.
[10]. Beurskens, M.N.A. et al., Physics of Plasmas **18** (2011) 056120.
[11]. Walk, J. R. et al., Nuclear Fusion **52** (2012) 63011.
[12]. Schnneider, P.A. et al., Plasma Physics and Controlled Fusion **54** (2012) 105009.
[13]. Kallenbach, A. et al., Journal of Nuclear Materials 337-339 (2005) 381.
[14]. Snyder, P.B. et al., Physics of Plasmas **16** (2009) 056118.
[15]. Groebner, R.J. et al., Nuclear Fusion **49** (2009) 085037.
[16]. Neu, R. et al., Submitted to PSI 2012 / Journal of Nuclear Materials .
[17]. Viezzer, E. et al., Review of Scientific Instruments **83** (2012) 103501.
[18]. Grierson, B.A. et al., Review of Scientific Instruments **81** (2010) 10D735.
[19]. Miller, R.L. et al., Physics of Plasmas **5** (1998) 973.
[20]. Connor, J.W. et al., Physics of Plasmas **5** (1998) 2687.
[21]. Maingi, R. et al., Physical Review Letters **103** (2009) 18.
[22]. Snyder, P. et al., Nuclear Fusion **44** (2004) 320.
[23]. Saarelma, S. et al., Plasma Physics and Controlled Fusion **51** (2009) 035001.
[24]. Fenstermacher, M. et al., Nuclear Fusion **45** (2005) 1493.
[25]. McCarthy, P.J., Plasma Physics and Controlled Fusion **54** (2012) 015010.
[26]. Dunne, M.G. et al., Nuclear Fusion **52** (2012) 123014.
[27]. Osborne, T.H. et al., Plasma Physics and Controlled Fusion **42** (2000) A175.
[28]. Snyder, P.B. et al., Physics of Plasmas **9** (2002) 2037.
[29]. Aiba, N. et al., Nuclear Fusion **52** (2012) 114002.

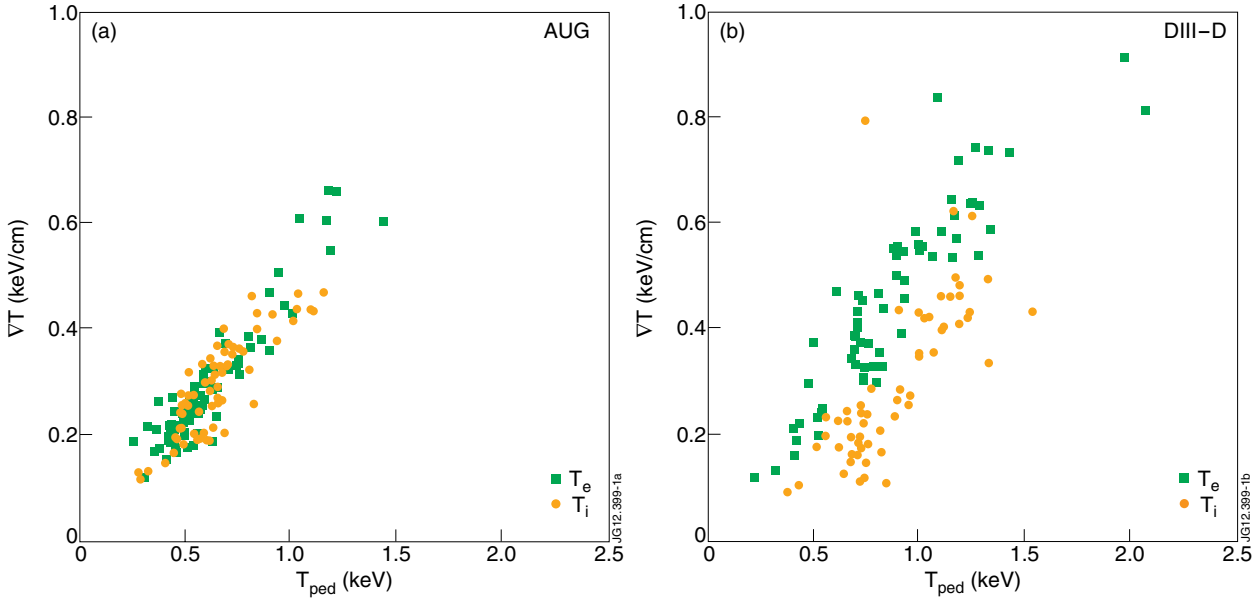

Figure 1: Pedestal gradient versus pedestal top temperature for electrons (green,square) and ions (orange,circle) with the discharges from AUG (a) and DIII-D (b).

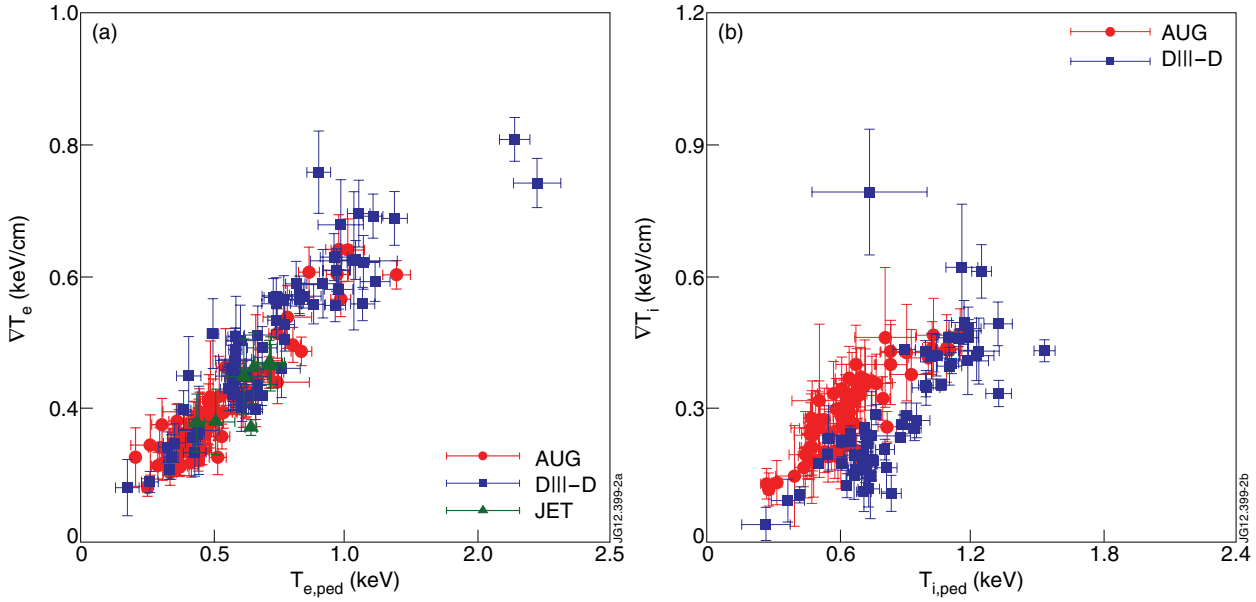

Figure 2: Mean real space gradient in the steep gradient zone of the pedestal plotted against the pedestal top value of electron temperature (a) and ion temperature (b).

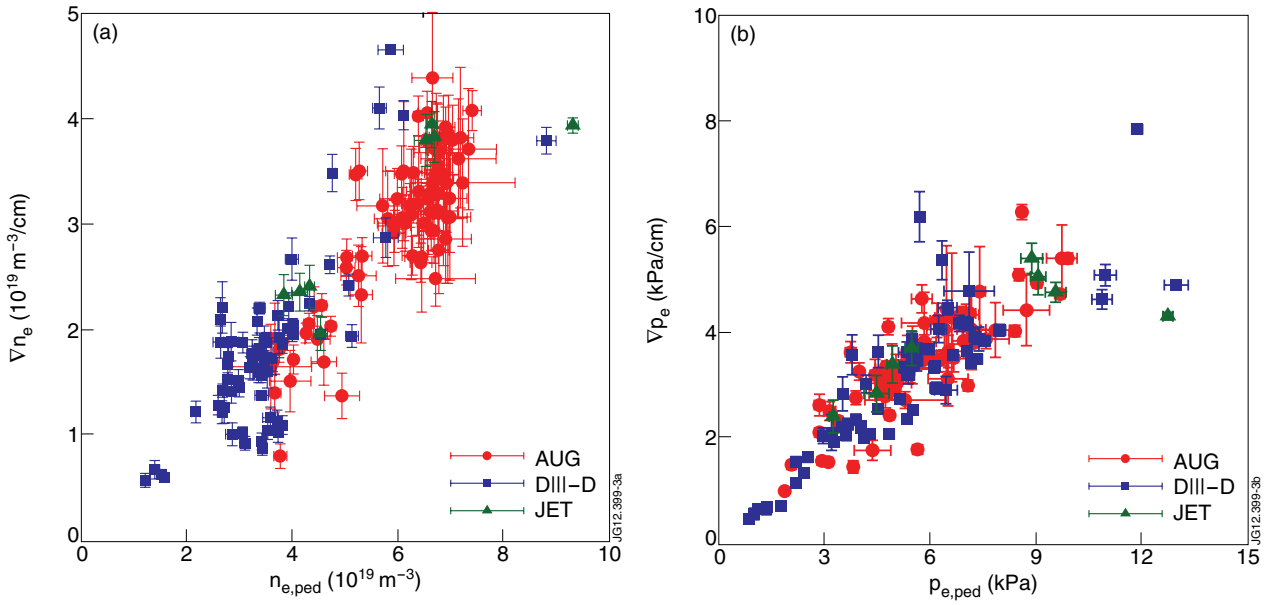

Figure 3: Mean real space gradient in the steep gradient zone of the pedestal plotted against the pedestal top value electron density (a) and electron pressure (b).

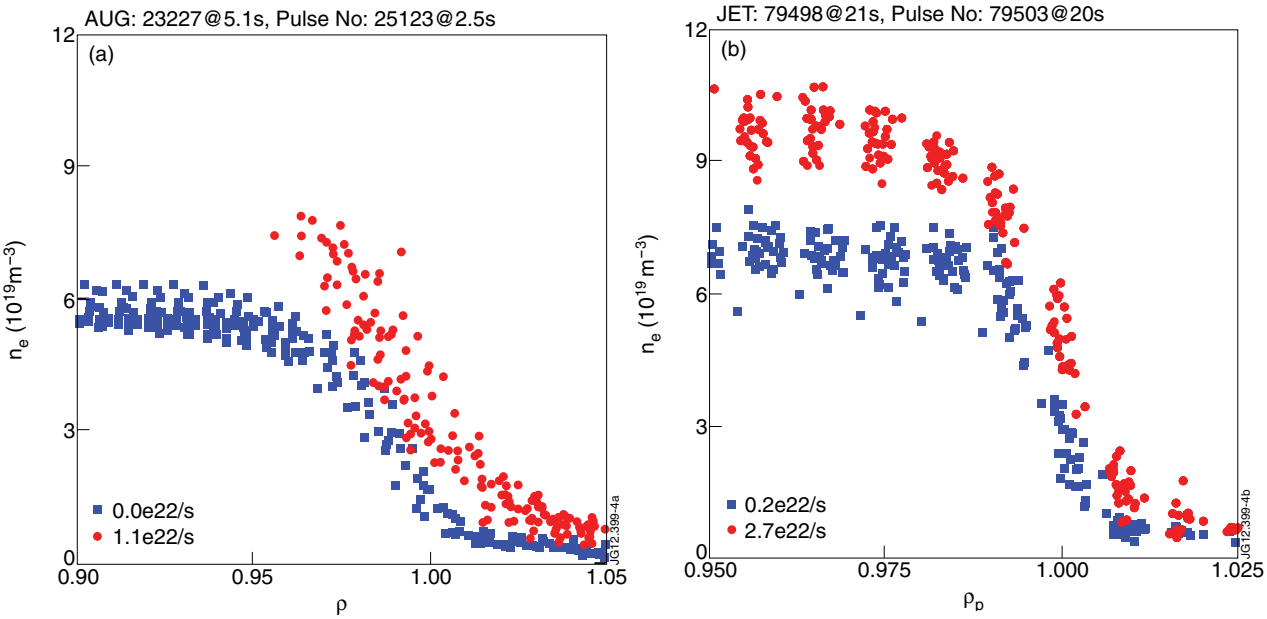

Figure 4: Electron density profiles at the edge for AUG (Li-Beam) (a) and JET (Thomson scattering) (b) with low (blue) and high (red) gas fuelling. The profiles are taken in an interval of 150ms (AUG) and 5s (JET) in a stationary plasma - the instrument function of the JET TS was taken into account. The pedestal top for the high density case at AUG is defined by an edge interferometer channel which is not plotted. The JET profile is plotted on a different range of the normalized radius to illustrate the comparable real space gradients.

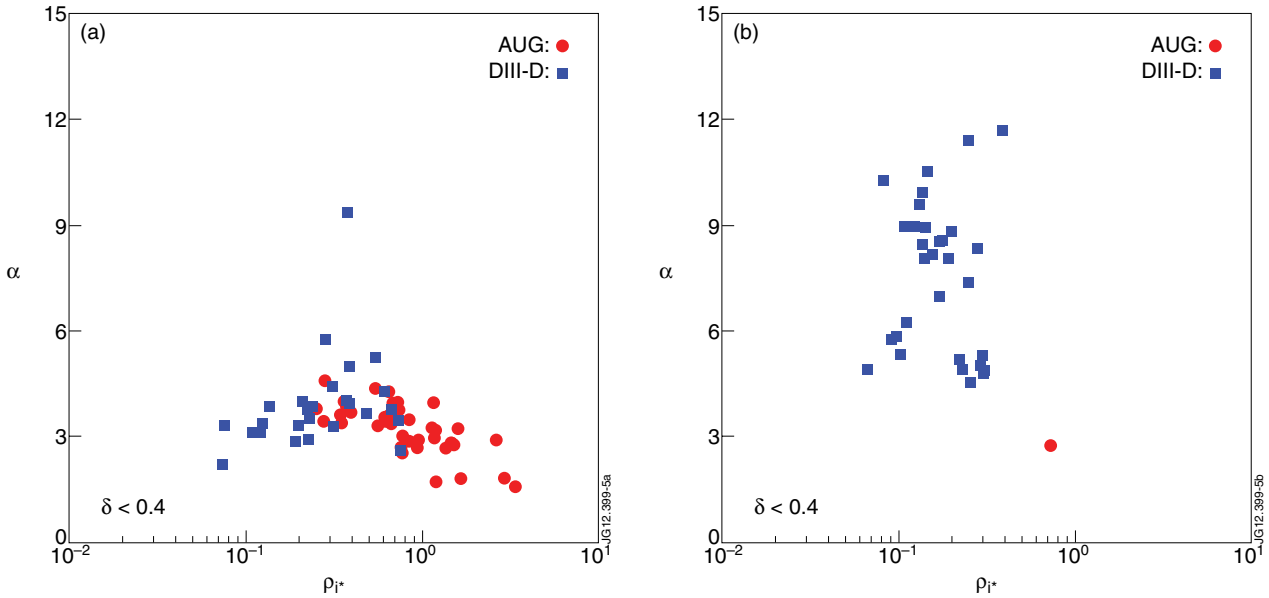

Figure 5: Normalized pressure gradient plotted against the collisionality for $\delta < 0.4$ *(a) and* $\delta > 0.4$.

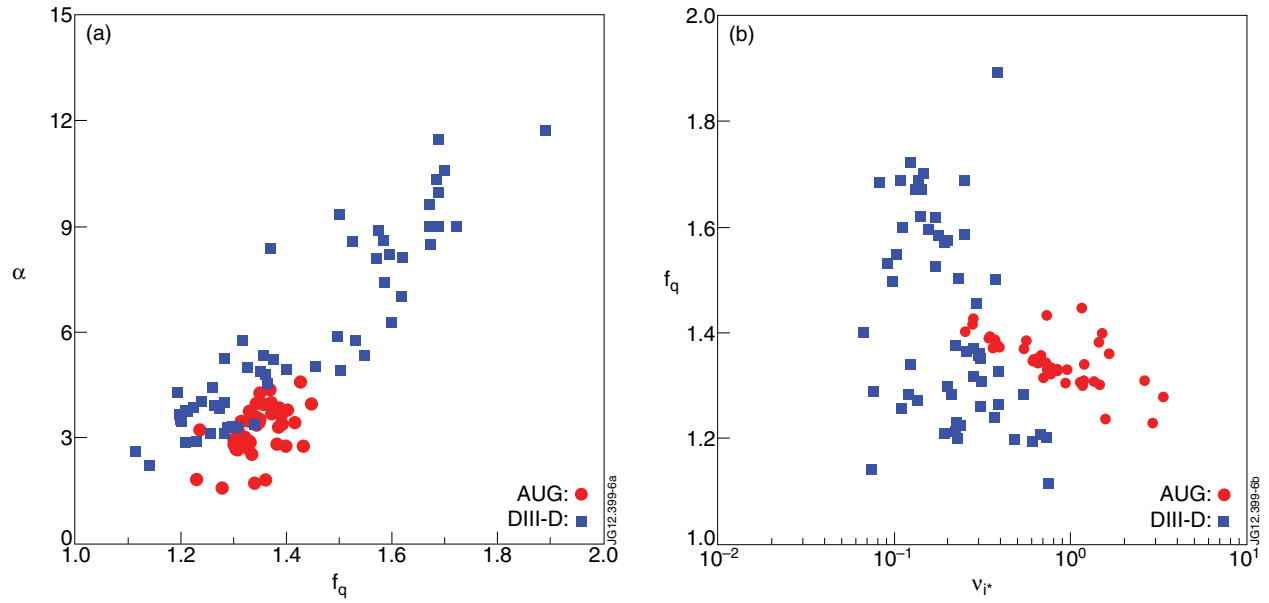

Figure 6: Normalized pressure gradient plotted against f_q *(a) and* f_q *plotted against collisionality*